https://doi.org/10.5194/nhess-2024-85
Preprint. Discussion started: 24 July 2024

Natural Hazards and Earth System Sciences
Discussions

From rockfall source areas identification to susceptibility zonation: a proposed workflow tested in El Hierro (Canary Islands, Spain)

Roberto Sarro[1*], Mauro Rossi[2], Paola Reichenbach[2], Rosa María Mateos[3]

[1] Department of Geohazards and Climate Change, Geological and Mining Institute of Spain (IGME-CSIC), Ríos Rosas 23, 28003, Madrid, Spain.
[2] Research Institute for Geo-Hydrological Protection (IRPI-CNR), Via Madonna Alta 126, 06128 Perugia, Italy.
[3] Department of Geohazards and Climate Change, Geological and Mining Institute of Spain (IGME-CSIC). Urb. Alcázar del Genil. Edificio Zulema, bajos, 18010 Granada, Spain.

**Correspondence to*: Roberto Sarro (r.sarro@igme.es)

Abstract. Accurate rockfall modeling is crucial for evaluating rockfall hazards and requires consideration of several inputs data, including parameters that control boulder trajectories and source areas. Inaccurate definitions of source areas can lead to unrealistic representations of the rockfall process. In this study, we analyze how different approaches used to define source areas can affect the accuracy of rockfall modeling. The island of El Hierro (Canary Islands, Spain) is selected due to its geological and geomorphological characteristics, as well as the socio-economic importance of rockfalls on the island.

To assess rockfall source areas, three different approaches were considered, ranging from situations with limited data availability to scenarios with many topographic, geological and geomorphological information.

A morphometric firstly approach establishes a slope angle threshold above which block detachment zones are considered. For the second approach, we have employed a statistical method to identify rockfall source areas, using Empirical Cumulative Distribution Functions (ECDF) of slope angle values. The third method was a probabilistic modeling framework that applies a combination of multiple multivariate statistical classification models. These models use the mapped source areas as a dependent variable, as well as a set of thematic information as independent variables.

The source area maps obtained from the three methods were used as inputs for a rockfall runout model, to establish a classification of rockfall susceptibility areas.

One of the main outcome of the rockfall modeling simulations on El Hierro is the rockfall trajectory counts maps, showing areas prone to rockfalls. These maps indicate the probability of a given pixel being affected by a rockfall event. Two classification approaches were applied to generate the probabilistic susceptibility maps: unsupervised and supervised statistical methods by using distribution functions. The unsupervised classification only employs as input the raster map of the rockfall trajectory counts. In contrast, the supervised classification requires additional data on the areas already affected by rockfalls. Finally, six susceptibility maps are developed and compared to highlight the influence of source areas definition on the distribution of rockfall trajectories.

https://doi.org/10.5194/nhess-2024-85
Preprint. Discussion started: 24 July 2024


Natural Hazards and Earth System Sciences Discussions

1 Introduction

Rockfalls are dangerous natural hazards with a relevant socio-economic impact worldwide (Borella et al., 2019; Mateos et al., 2020). Changes in environmental conditions related to the growth of the population, land-use intensification and industrial development have the potential to increase the impact of rockfalls in many different regions (Farvacque et al., 2019; Othman et al., 2021; Santangelo et al., 2020). In addition, climate change is expected to modify precipitation patterns with effects in the increasing frequency and extension of rockfalls (Gariano et al., 2015; Sarro et al., 2021). As a consequence, there is an increasing interest for improving the reliability and accuracy of tools and products able to support rockfalls management and mitigate their impact (Noël et al., 2021; Omran et al., 2021; Santos et al., 2024).

Rockfall runout models allow to obtain information on the spatial distribution of the boulders trajectories, their velocity, energy and heights (Carlà et al., 2019; Gallo et al., 2021), and play a relevant role in rockfall assessment, supporting the identification of rockfall-prone areas and the characterization of blocks behavior (Crosta et al., 2015; Pfeiffer, 2019). In the literature, different modeling approach were proposed based on data availability, environmental setting, and type of analyses. An incomplete list comprises : STONE (Guzzetti et al., 2003; Sarro et al., 2020), RocPro3d (Sarro et al., 2018, 2014), Hy-Stone (Dinçer et al., 2016; Lanfranconi et al., 2020), RAMMS (Dhiman and Thakur, 2021), RokyFor3D (Francioni et al., 2020; Robiati et al., 2019) and Rocfal (Kakavas et al., 2023; Pérez-Rey et al., 2019). The output of runout models are commonly used to estimate the rockfall susceptibility degree by classifying rockfall trajectories counts (Dorren et al., 2023; Nanehkaran et al., 2022; Noël et al., 2023).

Rockfalls simulation models, both probabilistic or deterministic, present errors associated with the input data employed to replicate the rockfall process (Straub and Schubert, 2008). The inaccuracy in defining rockfall sources areas is highly relevant in modeling, since source areas provide the starting state for rockfall trajectories (Frattini et al., 2013; Rossi et al., 2020).

The placement of source areas depends on several characteristics, such as slope morphology, lithology, and discontinuities (Alvioli et al., 2021; Sarro et al., 2018; Yan et al., 2023). At the local scale, in situ analyses commonly involve discontinuity characterization and escarpment recognition. Frequently, logistical and safety issues in the field constrain these methods. Remote sensing techniques, such as laser scanners and UAV-based photogrammetry, are nowadays widely used to address these limitations and obtain detailed observations of slopes (Gallo et al., 2021; Giordan et al., 2020; Sarro et al., 2018). Although both, fieldwork and remote sensing methods are successful at a local scale, their utility at a regional scale is limited. Many methods with different degrees of complexity have been proposed for identifying rockfall source areas at regional scale, based on deterministic, probabilistic or statistical approaches (Muzzillo et al., 2018). Most of them are based on the numerical analysis of digital elevation models (DEMs) and additional environmental dataset. Source areas can be identified analysing local topography by using surface slope thresholds, which denotes the area with the favourable conditions to boulder detachment. Larcher et al. (2012) proposed an equation for defining rockfall source areas by linking the slope angle threshold and the resolution of DEM. Rockfall source areas can also be identified empirically or derived from the decomposition of slope frequency distributions, using morphometric methods based on the slope angle thresholds. Several studies determined a

https://doi.org/10.5194/nhess-2024-85
Preprint. Discussion started: 24 July 2024


Natural Hazards and Earth System Sciences
Discussions

correlation between this threshold and the angle of internal friction of the rock massif (Loye et al., 2008; Paredes et al., 2015). Thus, the evaluation of slope frequency distributions can determine the angle of internal friction associated with each lithological unit of the rock massif, and it is used as the threshold beyond the block-rock becomes unstable. In the same way, Loye et al. (2009) developed a model based on the Gaussian distribution of the slope angle values. According to the result of this slope angle distribution, for each morphological unit, the steepest slopes are selected as potential source areas (Zhan et al., 2022). Additionally, Wang et al. (2021) identify rockfall source areas controlled by rock mass strength and by using relief-slope angle relationships.

Other identification techniques at regional scale are based on the analysis of remote sensing multi-temporal imagery, such as interpretation of orthophotos from optical aerial or satellite data. The use of distinctive imaging features/signs, as scars or deposits, has shown to be feasible in several researches (Liu et al., 2020; Mateos et al., 2016; Scavia et al., 2020). However, this technique is limited by the availability of satellite data, and the difficulty of analysing some areas (shadowed slopes, steep slopes and/or vegetation). Moreover, photo-interpretation is time-consuming and this often hampers its application over large areas (Alvioli et al., 2021).

Recently, advanced heuristic methods and statistical tools were proposed to identify the location of source areas with good results. A heuristic method depends on the site characteristics and its application requires validation and special adaptation processes (Fernandez-Hernández et al., 2012). Conversely, statistical methods can be performed to assess different levels of likelihood based on geomorphological, geological and some geo-environmental factors. These methods, such as multivariate analysis, logistic regression, or frequency ratio, are more flexible than heuristic methods, but require training with representative data samples. Hybrid methods combine statistical and experimental methods, such as neural networks or machine learning decision analysis, to reduce the amount of data required and improving the accuracy of the results (Fanos and Pradhan, 2019; Rossi et al., 2020).

In the literature, there are no specific studies that analyse how the goodness of source areas delimitation influence the rockfall modeling results. For this, this work analyses, for the first time and at a regional scale (EL Hierro, Spain), the effect of different methods to identify the source areas in the results of the rockfall modeling. Three types of approaches are considered for defining source areas, depending on data availability scenarios. Different source area maps are used as input data to rockfall runout model, which outputs are classified to derive rockfall susceptibility zonation. Finally, we discuss the type of classification developed (i.e., supervised versus unsupervised methods).

The article is organized in some sections. Section 2 describes the test area; Section 3 presents the variety of methodologies employed; Section 4 presents the results and, finally, Section 5 discusses the results and highlights the main conclusions.

https://doi.org/10.5194/nhess-2024-85
Preprint. Discussion started: 24 July 2024


Natural Hazards and Earth System Sciences Discussions

2 Test site and data

2.1 Geographical and geological setting

The Canary Islands is a volcanic archipelago located in the Atlantic Ocean, within the African plate. The archipelago is made up of seven major islands and some smaller ones which, together with underwater reliefs form an extensive volcanic domain. The islands are the result of a long magmatic history that started 70 million years ago and continues to the present day with the recent volcanic eruption in La Palma (September 2021).

El Hierro is the westernmost and the youngest island with an extension of 268.71 km^2 and a population of 11,147 inhabitants (Instituto Canario de Estadística, ISTAC, 2021). The climate is subtropical oceanic along the coast, very mild and sunny for most of the year, with rainfall concentrated from October to March. Heavy storms are frequent, associated with intense rainfall and strong winds that often trigger landslides. The average temperature ranges between 19 and 25ºC, with maximum values in August.

The morphology of the island is the result of numerous volcanic events, associated with important geological features. One of the most characteristic features of El Hierro is the presence of large landslides, which correspond to the escarpments of El Golfo, El Julan and Las Playas, located in the N, SW, and SE respectively. In the northern part, El Golfo, with cliffs that reach an elevation of more than 1,100 m, is a hazardous area for rockfalls. During the period 2011-2012, a submarine eruption took place about 2.5 km from the coastal village of La Restinga. The highest seismicity was in the El Golfo area, with two earthquakes of magnitude 4.4 and 4.6 in mid-November 2011. The seismic events triggered rockfalls near the Los Roquillos tunnel, one strategic infrastructure, which connects the municipalities of Frontera and Valverde, the most populated villages on the island.

After the event, the first field observations in the area carried out by technicians of the Geological and Mining Institute of Spain (IGME-CSIC), allowed to evaluate the cliff stability along the road HI-5, where the Roquillos tunnel is located. The report prepared showed a complex scenario for the analysis of rockfall hazard and the definition of source areas. The field surveys revealed that dykes that outcrop on the escarpments of the large landslides of El Golfo and Las Playas are preferential rockfall source areas. Recently, on 14 March 2021, a large rockfall along the El Golfo escarpment alerted the population and caused social alarm.

2.2 Available data and products

In this paper, we combine thematic data and products to identify source areas and to perform rockfall modelling and susceptibility zonation. To define the source areas, we have considered the following information: (1) morphometric parameters (elevation, slope, and curvature) derived from the Digital Elevation Model (DEM) with a resolution of 5m x 5m (Centro de Descargas del CNIG (IGN)); (2) lithological information from the geological map provided by IGME-CSIC, at a scale of 1:25000 and (3) some geomorphological information.

https://doi.org/10.5194/nhess-2024-85
Preprint. Discussion started: 24 July 2024


Natural Hazards and Earth System Sciences Discussions

Lithologies shown on the geological map were categorized into 5 geotechnical classes (Sarro et al., 2020; Rossi et al., 2020), ranging from class 1, which includes soft soils (such as lapilli and sand), to class 5, which includes very hard rocks (dikes, volcanic breccias, and massive basalts). From field observations, rockfall source areas in El Hierro are mainly related to hard and very hard rocks.

To classify and validate the simulated rockfall runout, we have prepared a map (Figure 1) that shows two types of areas: (1) (red polygons) areas affected by rockfalls where we have identified detached boulders by field investigation, aerial images and MOVES database (BDMoves); and (2) (green polygons) areas with no evidences of rockfall activity determined by a heuristic analysis taking into account field observations and geomorphological and topographical maps.

3 Methodology

To evaluate the influence of different source areas, to model rockfall and to assess the related susceptibility, we adopted a procedure based on the following steps: (i) identification of rockfall source areas using three different approaches, (ii) rockfall simulations, and (iii) classification of rockfall runout maps, their comparison and validation.

3.1 Identification of rockfall source areas

A crucial input for the rockfall analysis is the map of the source areas that we identified using three different approaches: (i) a morphometric schema based on the slope thresholding; (ii) the use of Cumulative Distribution Functions (CDF) that consider slope information and geology; and (iii) a probabilistic model (Figure 2 a, b, c).

3.1.1 Slope thresholding

The method (hereafter referred as ST_{RSA}) relies on a simple morphometric approach, which identifies as potential rockfall detachment zones, those areas with a slope angle above a given threshold. Even though, rockfall initiate mainly on steep slopes and steepness of the hillslope surface can be used to identify potential source areas. It is more realistic to determine a slope threshold using distinctive evidence (e.g. deposits, inventory) rather than arbitrarily establishing one (Michoud et al., 2012). According to Fu et al. (2021), more than 80% of 2238 rockfall records collected in Sichuan (China) over the past 30 years occurred on hillslopes with slope ranging between 30º and 50º, and most of them around 40º. As a result of an historical rockfall study in the Yosemite Valley (California, USA), Guzzetti et al. (2003) identified as potential release points, slopes above 60º. In the region of the County de Vaud (Switzerland), Jaboyedoff and Labiouse (2011) determined slope thresholds between 47º and 54º. Frattini et al. (2008), based on the experience of the Trentino Geological Survey, selected as source areas cells with slope angle over 37º in Val di Fassa (Dolomites, Eastern Italian Alps). Overall, most of the cited previous studies reveal slope thresholds over 30º.

https://doi.org/10.5194/nhess-2024-85
Preprint. Discussion started: 24 July 2024


Natural Hazards and Earth System Sciences Discussions

Sarro et al. (2020) proposed a slope threshold over 40º in Gran Canaria (Canary Islands), an island with similar topographical and geological conditions than El Hierro. Detailed evaluations revealed that source areas in Gran Canaria are mainly associated with hard, very hard, and extremely hard rocks.

The source area map obtained using the slope thresholding method is a binary map, where "0" corresponds to stable areas and "1" to rockfall prone detachment areas.

3.1.2 Statistical identification of rockfall source areas using slope angle ECDF

For the first statistical identification of rockfalls source areas, we exploited the Empirical Cumulative Distribution Functions (ECDF) of slope angle values (hereafter referred as CDF_{RSA}).

An ECDF function returns the probability that a random variable is less than or equal to a given value (Lee et al., 2022). In mathematical terms this is expressed by Equation 1:

$$F_x(x) = P(X \leq x) = \sum_{t \leq x} f(t) \qquad \text{Equation 1}$$

where $F_X(x)$ denotes the CDF of a random variable X whose probability distribution is f(x).

ECDF has a lower and upper limit respectively of 0 and 1 and gives a cumulated probability, which increases with the x value. Equation 2 shows the values taken by ECDF or $F_X(x)$ for infinite boundaries of the random variable, and Equation 3 the relation between $F_X(x)$ values for successive values of x.

$$F_x(-\infty) = 0, F_x(\infty) = 1 \qquad \text{Equation 2}$$

$$\forall x_{n+1} \geq x_n, F_x(x_{n+1}) \geq F_x(x_n) \qquad \text{Equation 3}$$

In our study, we selected the slope value as the random variable X, and using a supervised approach, we analysed only the slope values in correspondence of mapped rockfalls detachment areas to derive CDF_{RSA}. Thus, CDF_{RSA} gives the probability that the slope in rockfall source areas is less than or equal to a given value. This function represents the cumulative probability of slope to cause rockfalls and can be used as a quantitative probabilistic estimation of rockfall detachment for given slope values. The source areas map obtained using CDF_{RSA} approach is a probabilistic map, with values ranging from 0 to 1, respectively for a nil or unitary probability of being a potential rockfall detachment area.

3.1.3 Probabilistic identification of rockfall source areas using LAND-SUITE

The third method for the rockfall source areas identification (hereafter referred as $PROB_{RSA}$) proposes a probabilistic modelling framework that applies a combination of multiple multivariate statistical classification models, using the source area locations mapped in the field as dependent variable and a set of thematic data as independent variables (i.e., morphometric data derived from DEMs and lithological data). The model uses in input morphometric parameters derived from the Digital Elevation Model and lithological data as an expression of the mechanical behaviour of the rocks.

https://doi.org/10.5194/nhess-2024-85
Preprint. Discussion started: 24 July 2024


Natural Hazards and Earth System Sciences Discussions

As described in detail in Rossi et al. (2020), we applied the probabilistic framework using LAND-SUITE (LANDslide - Susceptibility Inferential Tool Evaluator) an R-based open source program (Rossi et al., 2022). The software allowed us to obtain a probabilistic source area map, which expresses the probability that a certain area could be a potential rockfall source area. A logistic regression model integrated into the tool was used for the preliminary analysis of different training/validation scenarios to determine whether the model was sensitive to the selection of dependent variables and to identify the best model training configuration for application on the island. Furthermore, the final source area zonation was carried out, enabling the combination of different statistical modelling approaches such as Linear Discriminant Analysis, Quadratic Discriminant Analysis, and Logistic Regression Model. Then, different LAND-SUITE tools were used to evaluate probabilistic source area maps that resulted from different model applications and configurations, to verify the modelling performance and to estimate the associated uncertainty. The resulting probabilistic source area zonation was evaluated by integrating the output expressing the variation for a variety of probability thresholds. Specifically, contingency matrices and plots along with model sensitivity, specificity, Cohen's kappa indices and ROC curves with the corresponding area under curve (AUC_{ROC}) values, were used to compare the observed and modelled source areas and to explore quantitatively the performances of different model configurations allowing the selection of the best model and the corresponding probabilistic source area map (Rossi et al., 2020).

Similarly, to the previous identification approach, the source areas map obtained using the method implemented with LAND-SUITE is a probabilistic map, with values ranging from 0 to 1, respectively for a nil or unitary probability of being a potential rockfall detachment area.

3.2 Deterministic rockfall runout simulation

The rockfall runout simulation was performed using a physically based model employing in input the three source areas maps described above. Such type of model is based on the fundamental principles of mass and energy conservation and is extensively employed worldwide to study the occurrence of rockfalls. In the context of rockfall hazard assessment, some parameters associated with the terrain and rock massif settings are used to compute the spatial distribution of trajectories, velocities, and heights.

In this study, we used STONE, a distributed 3-dimensional software based on physically based simulations. The software is raster based and applies a lumped mass approach to simulate boulder movement along a topography described by a Digital Elevation Model (Guzzetti et al., 2002).

The software requires four main inputs: (i) a digital elevation model, (ii) three coefficients maps (i.e., dynamic rolling friction, normal energy restitution, and tangential energy restitution) that simulate energy loss by a boulder when rolling and bouncing at impact points, (iii) a map portraying the location of the rockfall source areas, and (iv) a map of the number of simulations to be run during modelling. The main output is a raster map of the cumulative count of rockfall trajectories, along with additional maps of simulated boulder heights and velocities not used in this study.

https://doi.org/10.5194/nhess-2024-85
Preprint. Discussion started: 24 July 2024


Natural Hazards and Earth System Sciences Discussions

The three maps of model coefficients were estimated considering different lithological/geotechnical categories reported in the geotechnical map of El Hierro and selecting values reported for similar lithologies in the literature (Alvioli et al., 2021; Guzzetti et al., 2003; Mateos et al., 2016; Sarro et al., 2020).

The number of simulations run for each source area pixel was obtained multiplying the binary (i.e., 0 or 1) or probabilistic (i.e., from 0 to 1) value of the source area maps by 10, successively rounded to the closest integer value.

The main output of the runout modelling computed for each source area identification approach (Figure 2 a, b, c) is the cumulative frequency of rockfall trajectories counts (Figure 2 d, e, f).

3.3 Classification of rockfall runout for susceptibility estimation, model comparison and validation

The map of the rockfall trajectory counts estimates the potential of a specific pixel to be impacted by a rockfall. To generate a probabilistic susceptibility map, we employed two classification approaches based on the ECDF of trajectories counts and considering, respectively, an unsupervised and a supervised method.

The first approach uses an unsupervised classification technique and it is based exclusively on the raster map of rockfall trajectory counts. This method classifies the map of trajectories counts by utilizing the ECDF derived from the values of counts obtained in the entire study area by the rockfall runout model (i.e., cells with count value equal to or greater than 1). The resulting map is probabilistic with values ranging from 0 to 1 and shows a probabilistic estimation of the likelihood of a given pixel being affected by a rockfall.

The supervised classification method works similarly, but in such case the ECDF accounts only the trajectories counts in correspondence of rockfall deposits (i.e., rockfall talus) mapped in the study area (i.e., red polygons in Figure 1).

This twofold classification methodology was applied to the three maps of trajectories counts obtained by STONE and using as input the three source areas maps (i.e., ST_{RSA}, CDF_{RSA} and $PROB_{RSA}$). As a result, we obtained 6 ECDFs graphs and 6 different susceptibility maps.

To compare the final classified susceptibility maps, we set up different analyses. The six susceptibility maps were evaluated pairwise considering the three source area maps, and the two classification methods. To investigate and quantify the diversities, we used maps of the differences and histograms that enables the identification of the locations where the susceptibility maps show a greater (or a lower) likelihood of rockfall occurrence. Additionally, 2D hexagonal bin count heat maps derived for the different coupling of susceptibility maps, were plotted to show the correlation between the different model outcomes.

To validate the models, we used two rockfall inventories: (i) a polygon-type inventory with zones reached by rockfall boulders and zones without any significant evidence of potential boulders reaches; (ii) a point-type inventory with locations of isolated rockfall boulders at their final reach after runout (i.e., silent witnesses). We first used the polygon-type inventory to derive ROC plots (Rossi et al., 2022, 2010; Rossi and Reichenbach, 2016) and the corresponding area under curve (AUC_{ROC}) with the main purpose of showing the differences between the modelled and observed susceptibility values and providing a quantitative estimates of the final rockfall susceptibility zonation performances, regardless the adopted classification approach. Successively, we analysed the distribution of average susceptibility values (i.e., violin plots) within circular buffers of different

https://doi.org/10.5194/nhess-2024-85
Preprint. Discussion started: 24 July 2024


Natural Hazards and Earth System Sciences Discussions

sizes built around boulders locations reported in the point-like inventory, to verify the capability of models to discriminate susceptible conditions in correspondence and in the vicinities of mapped rockfall boulders.

4 Results

4.1 Comparison of different source areas maps

Following the steps of the methodology, we first compared the source areas maps prepared using three different approaches (see section §3.1). The three maps cover the entire island with consistent and equal spatial coverage.

Using the morphometric approach based on slope thresholding (ST_{RSA}), we determined a threshold of 40º by combining geomorphological data, geological analysis and historical rockfall events. In this case, for the entire island, a total of 727,603 pixels were identified as prone to rockfalls detachment, corresponding to 18.19 km^2 (6.8% of the island, Table 1). To carry out the rockfall simulation, the binary value was multiplied by 10, resulting in two values: 10 simulations in correspondence of rockfall source areas and 0 elsewhere.

In the second approach, we used CDF_{RSA} to obtain a probabilistic source map with values ranging from 0 to 1, respectively for a nil or unitary probability of being a potential rockfall detachment area. Unlike the binary values in the ST_{RSA} map, this probabilistic information allows to identify the source areas with different levels of certainty. The map shows that 1,628,048 pixels have not- nil probability of being a potential detachment area, twice the number of pixels identified with the binary approach (ST_{RSA}). Source areas identified through CDF_{RSA} cover a total area of 40.70 km^2, around 15% of the island's surface. In this case, the map of the number of runout simulations has integer values ranging from 0 to 10, differently from ST_{RSA}.

The third source area probabilistic map obtained with the $PROB_{RSA}$ method shows a total of 3,339,686 pixels with not nil probability of being a potential detachment area, which is equivalent to 84.99 km^2, approximately the 31.6% of the entire island surface. Similarly, to the CDF_{RSA} case, the resulting map of the number of simulations has integer values ranging from 0 to 10.

The comparison of source areas identified with the three methods was performed using spatial overlay in raster format and frequency-based criteria.

The three maps show a diversified spatial arrangement of the pixels identified as rockfall source areas (Figure 3). A total of 727,423 pixels were recognized as source areas through the three different methods, with the matching areas mostly located on steep slopes (Figure 3, dark blue pixels). No pixels were identified as source area only by ST_{RSA} being always associated with either CDF_{RSA} or $PROB_{RSA}$. The pixels identified only by $PROB_{RSA}$ are 1,855,918, corresponding to more than 55% of the pixels identified with other methods or methods combinations.

The comparison between the source area maps shows that only 727,423 pixels are classified as source areas by the three approaches (Table 2). ST_{RSA} is always predicting source areas jointly to another method. The largest source area match is observed between CDF_{RSA} and $PROB_{RSA}$, with a number of pixels of 816,278 (20.40 km^2), while the largest mismatch for ST_{RSA} and $PROB_{RSA}$, with a deviation of 2,672,196 (66,80 km^2) pixels detected by $PROB_{RSA}$ but not by ST_{RSA}. This provides

https://doi.org/10.5194/nhess-2024-85
Preprint. Discussion started: 24 July 2024


Natural Hazards and Earth System Sciences Discussions

evidence that the $PROB_{RSA}$ tends to be more conservative when identifying source areas, covering a larger portion of the study area (1,855,918 pixels and 46,39 km^2).

Furthermore, Table 2 shows the differences in the spatial distribution of source areas identified by the three approaches, both in terms of pixels and square kilometres, highlighting the results that stem from employing these methods. According to Figure 3, it is evident that the ST does not have as much significance in the differences as the other approaches.

Table 2 also includes the geotechnical classes proposed by (Rossi et al., 2020)) and classifies them as source areas. It is evident that the discrepancies between the ST_{RSA} and the other approaches (CDF_{RSA} and $PROB_{RSA}$) correspond to classes not associated with rockfall source areas, such as soft and hard soils.

4.2 Comparison of rockfall simulation and susceptibility maps

The output of run-out simulation obtained by STONE (Figure 2 d, e, f), using as input the different source areas maps (i.e., ST_{RSA}, CDF_{RSA} and $PROB_{RSA}$), show diversified spatial distributions of rockfall counts providing a potential different information on the susceptibility posed by rockfall in the study area. To address this diversity, we have proposed to classify the trajectories count maps using two approaches based on unsupervised and supervised ECDF analysis (Figure 4 and Figure 5).

The comparison of the trajectory maps with the simplified geotechnical classes map (Figure 1 in (Rossi et al., 2020)) reveals that the rockfall trajectories mainly involve lithology types classified as “very hard rocks” and “hard rocks”, whereas trajectories through “soft rocks” are quite limited.

Areas characterized by “very hard rock” are affected by rockfalls trajectories of unsupervised classification maps for approximately 19%, 25% and 42% corresponding to ST_{RSA}, CDF_{RSA}, and $PROB_{RSA}$, whereas for “hard rocks” areas, the percentages decrease to 7%, 17% and 37%.

These percentages can be explained by the geological and morphological setting. Furthermore, the "hard soil" class also shows considerable percentages, above 70%. This distribution pattern aligns with their position in the lower part of slopes, where trajectory paths commonly stops. However, the trajectories do not pass through areas with “soft soil”, which are primarily located in flat terrain.

For the supervised maps, the analysis of the runout simulations reveals that "very hard rock" and "hard rock" classes are affected by trajectories for 81%, 81%, and 88%, respectively.

The analysis of unsupervised (Figure 5 a, b, c) and supervised (Figure 5 d, e, f) ECDF generally shows a different behaviour. The unsupervised distributions show larger ranges and higher number of cells with low trajectories counts (i.e., values close to 0). The comparison of the unsupervised ECDFs (Figure 5 a, b, c) reveals a larger number of cells with high count values for ST_{RSA}, followed by $PROB_{RSA}$ and CDF_{RSA}. With this behaviour reversed when considering supervised ECDFs (Figure 5 d, e, f).

The application of the ECDFs (i.e., derived for different runout models taking in input different source area maps) to the relative trajectories’ count maps, allows to derive the six probabilistic susceptibility maps shown in Figure 4. This figure shows

https://doi.org/10.5194/nhess-2024-85
Preprint. Discussion started: 24 July 2024

larger differences between the 3 maps for the different source area using the unsupervised ECDFs (Figure 4 a, b, c); such differences are reduced/minor when considering the supervised alternatives (Figure 4 d, e, f).

Figure 6 and Figure 7 show the pairwise difference of susceptibility maps obtained using different source area maps and diversified classification method. Specifically, the figure portraits the following six pairs of results: (a) $ST_{RSA\text{-}unsup}$-$CDF_{RSA\text{-}unsup}$, (b) $ST_{RSA\text{-}unsup}$-$PROB_{RSA\text{-}unsup}$, (c) $CDF_{RSA\text{-}unsup}$-$PROB_{RSA\text{-}unsup}$, (d) $ST_{RSA\text{-}sup}$-$CDF_{RSA\text{-}sup}$, (e) $ST_{RSA\text{-}sup}$-$PROB_{RSA\text{-}sup}$, and (f) $CDF_{RSA\text{-}sup}$-$PROB_{RSA\text{-}sup}$. The lighter colours (i.e., lower absolute difference values) between supervised maps pairs and the frequency counts of the corresponding histograms, highlight lower differences between the susceptibility outputs obtained applying supervised ECDFs.

The 2D hexagonal bin count heat maps (Figure 8), derived for the different pairs of susceptibility maps, confirm these results showing a better alignment along the bisector of the higher frequency counts (i.e., dark reddish hexagons) obtained for supervised susceptibility maps (Figure 4 d, e, f).

4.3 Rockfall susceptibility model validation

Figure 9 shows the results of the ROC analysis comparing the six susceptibility maps of Figure 4 and rockfall field observations. The graphs show that the model with the best performance is obtained by using the $PROB_{RSA}$ source areas (AUC_{ROC}=0.88), followed by the CDF_{RSA} (AUC_{ROC}=0.84).

For the same susceptibility maps, Figure 10 shows the distributions of the average values within circular buffers of 5m, 50m and 100m defined around observed boulders locations. Susceptibility average and maximum values increase with the decrease of the buffer size. The distributions of values change significantly for different source areas when the susceptibility is classified using the unsupervised EDCF, whereas they tend to be more homogeneous when the supervised ECDF is applied.

5 Conclusions

Rockfall modeling is complex and requires a set of dedicated methodological choices and assumptions. Despite specific aspects of modeling have been largely discussed in the literature (Ding et al., 2023; Noël et al., 2023; Yan et al., 2023; Yang et al., 2021; Žabota et al., 2019), a comprehensive methodology to assess susceptibility posed by rockfalls (i.e., a key information for a proper hazard estimation) is still missing. To fulfil this gap, we have proposed a new workflow, which includes methods for the source area identification, the deterministic runout modelling, the classification of runout modelling output to derive objective rockfall probabilistic susceptibility zonation and the comparison and validation of the results. The methodology was applied in the island of El Hierro (Canary Islands, Spain), where rockfalls pose a significant threat to structures, infrastructures and population. We have presented three methods for identifying source areas of increasingly complexity, namely ST_{RSA}, CDF_{RSA} and $PROB_{RSA}$, which requires diversified input. Table 2 and Figure 3 show how these methods may lead to different spatial input maps (i.e., source area and number of simulation maps) for rockfall deterministic runout models, impacting the rockfall trajectories simulation and the corresponding susceptibility zonation (Figure 4).

https://doi.org/10.5194/nhess-2024-85
Preprint. Discussion started: 24 July 2024

To derive rockfall susceptibility maps, the trajectories values can be classified using different systems, including Equal Interval, Natural Break, Quantile, Standard Deviation, Head/Tail Breaks and Landslide Percentage (Alqadhi et al., 2022; Baeza et al., 2016; Cantarino et al., 2019; Tehrani et al., 2022; Wang et al., 2016).

We propose a methodological approach to derive probabilistic susceptibility maps based on the use of unsupervised and supervised ECDFs of the trajectories counts. We demonstrate with quantitative metrics (Figure 7 and Figure 8), how the use of the supervised ECDF approach helps reducing differences and homogenising zonation, at the expenses of a dedicated mapping effort to derive a rockfall inventory (Figure 1). This is a significant methodological finding of this work and shows that even using simple source areas identification methods, such as ST_{RSA} or CDF_{RSA}, supervised ECDF application guarantees an acceptable and not biased zonation of rockfall susceptibility maps.

This study also explores the strategies to validate the rockfall susceptibility model outputs, using different types of inventories, such as polygon-type maps portraying the zones reached by rock fall boulders and zones without any significant evidence of potential boulders' reaches, and point-type inventories showing only locations of isolated rockfall boulders at their final reach after runout (i.e., silent witnesses). Diffused metrics comparing modelled and observed values (i.e., ROC plots and correspondent AUC_{ROC}) can be used to show the performances of susceptibility models, regardless the adopted classification approach (Figure 9). Indeed, identical AUC_{ROC} values are obtained for unsupervised and supervised ECDFs, when the same source area identification method is used. The ROC analysis is sensitive to methodological choices and helped identifying $PROB_{RSA}$ (followed by CDF_{RSA} and ST_{RSA}) as the preferable method to identify rockfall source areas. Such results can be explained by the larger statistical robustness of this method (Rossi et al., 2020), which requires a dedicated mapping, a set of thematic information and the use of specific statistical software such as LAND-SUITE (Rossi et al., 2022). In general, we demonstrated that the larger is the effort in the identification of source areas, the more reliable and accurate is the rockfall susceptibility zonation.

When only rockfall point-type inventories are available, a simple analysis of the distribution of average susceptibility values, within circular buffers of different sizes (Figure 10) built around boulders locations, can provide a basic verification of the capability of models to discriminate susceptible conditions in correspondence and in the vicinities of the mapped/observed boulders. Such analysis also clearly shows the effect of using different classification approaches and confirms that the use of supervised ECDFs should be preferred as a method for generating comparable rockfall susceptibility zonation.

Despite different softwares and methods for rockfall runout simulation are available in the literature, we selected STONE that was already tested and used in the study area. However, we acknowledge that the rockfall modeling methodology proposed in this study holds even using different runout modelling approaches.

We conclude that the methodology here proposed provides guidance for an objective and reliable rockfall modelling to support civil protection, emergency authorities and decision makers in evaluating and assessing potential rockfall impacts. In addition, we believe that the entire approach can also be a strategic support for early rockfall warning systems.

https://doi.org/10.5194/nhess-2024-85
Preprint. Discussion started: 24 July 2024


Natural Hazards and Earth System Sciences Discussions

Code availability

LAND-SUITE V1.0 is archived in the Zenodo repository at https://doi.org/10.5281/zenodo.5650810 (Rossi and Bornaetxea, 2021).

Data availability

The authors can provide the El Hierro (Canary Islands, Spain) data used in the analyses to allow replication of the results.

Author contributions

Roberto Sarro: Conceptualization, Methodology, Investigation, Formal analysis, Validation, Writing - Original Draft, Visualization. Mauro Rossi: Conceptualization, Methodology, Software, Formal analysis, Validation, Writing - Original Draft, Visualization. Paola Reichenbach: Conceptualization, Methodology, Formal analysis, Validation, Writing - Review & Editing. Rosa María Mateos: Conceptualization, Methodology, Investigation, Formal analysis, Validation, Writing - Review & Editing. Given the contributions to the research all the authors should be consider as main authors.

Competing interests

The authors declare that they have no conflict of interest. At least one of the (co-)authors is a member of the editorial board of Natural Hazards and Earth System Sciences.

Acknowledgements

This work has been funded by the project U-GEOHAZ (Geohazard Impact Assessment for Urban Areas, Grant Agreement No. 783169) funded by the European Commission, Directorate-General Humanitarian Aid and Civil Protection (ECHO); and RISKCOAST project (Ref: SOE3/P4/E0868) funded by the INTERREG SUDOE program (3rd call for proposals). It was also partially supported by the University of Alicante in the framework of Quality Improvement Grant of PhD Program in Materials, Structures and Soil Engineering: Sustainable Construction.

References

Alqadhi, S., Mallick, J., Talukdar, S., Bindajam, A. A., Van Hong, N., and Saha, T. K.: Selecting optimal conditioning parameters for landslide susceptibility: an experimental research on Aqabat Al-Sulbat, Saudi Arabia, Environ Sci Pollut Res, 29, 3743–3762, https://doi.org/10.1007/s11356-021-15886-z, 2022.

https://doi.org/10.5194/nhess-2024-85
Preprint. Discussion started: 24 July 2024

Alvioli, M., Santangelo, M., Fiorucci, F., Cardinali, M., Marchesini, I., Reichenbach, P., Rossi, M., Guzzetti, F., and Peruccacci, S.: Rockfall susceptibility and network-ranked susceptibility along the Italian railway, Engineering Geology, 293, 106301, https://doi.org/10.1016/j.enggeo.2021.106301, 2021.

Baeza, C., Lantada, N., and Amorim, S.: Statistical and spatial analysis of landslide susceptibility maps with different classification systems, Environ Earth Sci, 75, 1318, https://doi.org/10.1007/s12665-016-6124-1, 2016.

Borella, J., Quigley, M., Krauss, Z., Lincoln, K., Attanayake, J., Stamp, L., Lanman, H., Levine, S., Hampton, S., and Gravley, D.: Geologic and geomorphic controls on rockfall hazard: how well do past rockfalls predict future distributions?, Natural Hazards and Earth System Sciences, 19, 2249–2280, https://doi.org/10.5194/nhess-19-2249-2019, 2019.

Cantarino, I., Carrion, M. A., Goerlich, F., and Martinez Ibañez, V.: A ROC analysis-based classification method for landslide susceptibility maps, Landslides, 16, 265–282, https://doi.org/10.1007/s10346-018-1063-4, 2019.

Carlà, T., Nolesini, T., Solari, L., Rivolta, C., Dei Cas, L., and Casagli, N.: Rockfall forecasting and risk management along a major transportation corridor in the Alps through ground-based radar interferometry, Landslides, 16, 1425–1435, https://doi.org/10.1007/s10346-019-01190-y, 2019.

Crosta, G. B., Agliardi, F., Frattini, P., and Lari, S.: Key Issues in Rock Fall Modeling, Hazard and Risk Assessment for Rockfall Protection, in: Engineering Geology for Society and Territory - Volume 2, edited by: Lollino, G., Giordan, D., Crosta, G. B., Corominas, J., Azzam, R., Wasowski, J., and Sciarra, N., Springer International Publishing, Cham, 43–58, https://doi.org/10.1007/978-3-319-09057-3_4, 2015.

Dhiman, R. K. and Thakur, M.: Rockfall Hazard Assessment Using RAMMS for the SE Facing Escarpment of Manikaran, Himachal Pradesh, India, in: Recent Technologies for Disaster Management and Risk Reduction: Sustainable Community Resilience & Responses, edited by: Rai, P. K., Singh, P., and Mishra, V. N., Springer International Publishing, Cham, 57–74, https://doi.org/10.1007/978-3-030-76116-5_4, 2021.

Dinçer, İ., Orhan, A., Frattini, P., and Crosta, G. B.: Rockfall at the heritage site of the Tatlarin Underground City (Cappadocia, Turkey), Nat Hazards, 82, 1075–1098, https://doi.org/10.1007/s11069-016-2234-z, 2016.

Ding, Y., Wu, Y., Zhu, Q., Zhang, L., Sun, Q., and Wang, W.: Virtual geographic environment-based integrated rockfall risk simulation method for canyon bridges, Transactions in GIS, 27, 797–820, https://doi.org/10.1111/tgis.13046, 2023.

Dorren, L., Schaller, C., Erbach, A., and Moos, C.: Automated Delimitation of Rockfall Hazard Indication Zones Using High-Resolution Trajectory Modelling at Regional Scale, Geosciences, 13, 182, https://doi.org/10.3390/geosciences13060182, 2023.

Fanos, A. M. and Pradhan, B.: A Novel Hybrid Machine Learning-Based Model for Rockfall Source Identification in Presence of Other Landslide Types Using LiDAR and GIS, Earth Syst Environ, 3, 491–506, https://doi.org/10.1007/s41748-019-00114-z, 2019.

Farvacque, M., Lopez-Saez, J., Corona, C., Toe, D., Bourrier, F., and Eckert, N.: How is rockfall risk impacted by land-use and land-cover changes? Insights from the French Alps, Global and Planetary Change, 174, 138–152, https://doi.org/10.1016/j.gloplacha.2019.01.009, 2019.

Fernandez-Hernández, M., Paredes, C., Castedo, R., Llorente, M., and de la Vega-Panizo, R.: Rockfall detachment susceptibility map in El Hierro Island, Canary Islands, Spain, Nat Hazards, 64, 1247–1271, https://doi.org/10.1007/s11069-012-0295-1, 2012.

https://doi.org/10.5194/nhess-2024-85
Preprint. Discussion started: 24 July 2024

Francioni, M., Antonaci, F., Sciarra, N., Robiati, C., Coggan, J., Stead, D., and Calamita, F.: Application of Unmanned Aerial Vehicle Data and Discrete Fracture Network Models for Improved Rockfall Simulations, Remote Sensing, 12, 2053, https://doi.org/10.3390/rs12122053, 2020.

Frattini, P., Crosta, G., Carrara, A., and Agliardi, F.: Assessment of rockfall susceptibility by integrating statistical and physically-based approaches, Geomorphology, 94, 419–437, https://doi.org/10.1016/j.geomorph.2006.10.037, 2008.

Frattini, P., Crosta, G. B., and Agliardi, F.: Rockfall characterization and modeling, in: Landslides, https://doi.org/10.1017/cbo9780511740367.023, 2013.

Fu, H., Chen, W., and Fu, J.: Rockfall mechanisms and block theoretical stability analysis, in: Rock Mechanics and Engineering, Elsevier, 89–125, https://doi.org/10.1016/B978-0-12-822424-3.00003-7, 2021.

Gallo, I. G., Martínez-Corbella, M., Sarro, R., Iovine, G., López-Vinielles, J., Hérnandez, M., Robustelli, G., Mateos, R. M., and García-Davalillo, J. C.: An Integration of UAV-Based Photogrammetry and 3D Modelling for Rockfall Hazard Assessment: The Cárcavos Case in 2018 (Spain), Remote Sensing, 13, 3450, https://doi.org/10.3390/rs13173450, 2021.

Gariano, S. L., Brunetti, M. T., Iovine, G., Melillo, M., Peruccacci, S., Terranova, O., Vennari, C., and Guzzetti, F.: Calibration and validation of rainfall thresholds for shallow landslide forecasting in Sicily, southern Italy, Geomorphology, 228, 653–665, https://doi.org/10.1016/j.geomorph.2014.10.019, 2015.

Giordan, D., Adams, M. S., Aicardi, I., Alicandro, M., Allasia, P., Baldo, M., De Berardinis, P., Dominici, D., Godone, D., Hobbs, P., Lechner, V., Niedzielski, T., Piras, M., Rotilio, M., Salvini, R., Segor, V., Sotier, B., and Troilo, F.: The use of unmanned aerial vehicles (UAVs) for engineering geology applications, Bull Eng Geol Environ, 79, 3437–3481, https://doi.org/10.1007/s10064-020-01766-2, 2020.

Guzzetti, F., Crosta, G., Detti, R., and Agliardi, F.: STONE: a computer program for the three-dimensional simulation of rock-falls, Computers & Geosciences, 28, 1079–1093, https://doi.org/10.1016/S0098-3004(02)00025-0, 2002.

Guzzetti, F., Reichenbach, P., and Wieczorek, G. F.: Rockfall hazard and risk assessment in the Yosemite Valley, California, USA, Nat. Hazards Earth Syst. Sci., 3, 491–503, https://doi.org/10.5194/nhess-3-491-2003, 2003.

Instituto Canario de Estadística, ISTAC [WWW Document], 2021. URL http://www.gobiernodecanarias.org/istac/ (accessed 12.5.22).

Instituto Geográfico Nacional, 2023. Centro de Descargas del CNIG (IGN) [WWW Document]. URL https://centrodedescargas.cnig.es/CentroDescargas/index.jsp

Instituto Geológico y Minero de España, 2023. BDMoves [WWW Document]. URL http://info.igme.es/BD2DMoves/)

Jaboyedoff, M. and Labiouse, V.: Technical note: Preliminary estimation of rockfall runout zones, Natural Hazards and Earth System Science, 11, 819–828, https://doi.org/10.5194/nhess-11-819-2011, 2011.

Kakavas, M. P., Nikolakopoulos, K. G., Kyriou, A., and Koukouvelas, I.: The Influence of the DSM Spatial Resolution in Rockfall Simulation and Validation with In Situ Data, Geosciences, 13, 57, https://doi.org/10.3390/geosciences13020057, 2023.

Lanfranconi, C., Sala, G., Frattini, P., Crosta, G. B., and Valagussa, A.: Assessing the rockfall protection efficiency of forests at the regional scale, Landslides, 17, 2703–2721, https://doi.org/10.1007/s10346-020-01458-8, 2020.

https://doi.org/10.5194/nhess-2024-85
Preprint. Discussion started: 24 July 2024

Larcher, V., Simoni, S., Pasquazzo, R., Strada, C., Zampedrio, G., and Berger, F.: PARAmount: WP6 guidelines, Rockfall and Forecast systems, 2012.

Lee, J.-J., Song, M.-S., Yun, H.-S., and Yum, S.-G.: Dynamic landslide susceptibility analysis that combines rainfall period, accumulated rainfall, and geospatial information, Sci Rep, 12, 18429, https://doi.org/10.1038/s41598-022-21795-z, 2022.

Liu, H., Wang, X., Liao, X., Sun, J., and Zhang, S.: Rockfall Investigation and Hazard Assessment from Nang County to Jiacha County in Tibet, Applied Sciences, 10, 247, https://doi.org/10.3390/app10010247, 2020.

Loye, A., Pedrazzini, A., and Jaboyedoff, M.: Regional indicative rockfall map using LIDAR based slope frequency histogram and conefall modelling, in: Interdisciplinary Workshop on Rockfall Protection: Morschach, Switzerland, Proceedings, 64–66, 2008.

Loye, A., Jaboyedoff, M., and Pedrazzini, A.: Identification of potential rockfall source areas at a regional scale using a DEM-based geomorphometric analysis, Natural Hazards and Earth System Science, https://doi.org/10.5194/nhess-9-1643-2009, 2009.

Mateos, R. M., García-Moreno, I., Reichenbach, P., Herrera, G., Sarro, R., Rius, J., Aguiló, R., and Fiorucci, F.: Calibration and validation of rockfall modelling at regional scale: application along a roadway in Mallorca (Spain) and organization of its management, Landslides, 13, 751–763, https://doi.org/10.1007/s10346-015-0602-5, 2016.

Mateos, R. M., López-Vinielles, J., Poyiadji, E., Tsagkas, D., Sheehy, M., Hadjicharalambous, K., Liscák, P., Podolski, L., Laskowicz, I., Iadanza, C., Gauert, C., Todorović, S., Auflič, M. J., Maftei, R., Hermanns, R. L., Kociu, A., Sandić, C., Mauter, R., Sarro, R., Béjar, M., and Herrera, G.: Integration of landslide hazard into urban planning across Europe, Landscape and Urban Planning, https://doi.org/10.1016/j.landurbplan.2019.103740, 2020.

Michoud, C., Derron, M.-H., Horton, P., Jaboyedoff, M., Baillifard, F.-J., Loye, A., Nicolet, P., Pedrazzini, A., and Queyrel, A.: Rockfall hazard and risk assessments along roads at a regional scale: example in Swiss Alps, Natural Hazards and Earth System Sciences, 12, 615–629, https://doi.org/10.5194/nhess-12-615-2012, 2012.

Muzzillo, R., Losasso, L., and Sdao, F.: Rockfall Source Areas Assessment in an Area of the Pollino National Park (Southern Italy), in: Computational Science and Its Applications – ICCSA 2018, vol. 10962, edited by: Gervasi, O., Murgante, B., Misra, S., Stankova, E., Torre, C. M., Rocha, A. M. A. C., Taniar, D., Apduhan, B. O., Tarantino, E., and Ryu, Y., Springer International Publishing, Cham, 366–379, https://doi.org/10.1007/978-3-319-95168-3_25, 2018.

Nanehkaran, Y. A., Licai, Z., Chen, J., Azarafza, M., and Yimin, M.: Application of artificial neural networks and geographic information system to provide hazard susceptibility maps for rockfall failures, Environ Earth Sci, 81, 475, https://doi.org/10.1007/s12665-022-10603-6, 2022.

Noël, F., Cloutier, C., Jaboyedoff, M., and Locat, J.: Impact-Detection Algorithm That Uses Point Clouds as Topographic Inputs for 3D Rockfall Simulations, Geosciences, 11, 188, https://doi.org/10.3390/geosciences11050188, 2021.

Noël, F., Nordang, S. F., Jaboyedoff, M., Digout, M., Guerin, A., Locat, J., and Matasci, B.: Comparing Flow-R, Rockyfor3D and RAMMS to Rockfalls from the Mel de la Niva Mountain: A Benchmarking Exercise, Geosciences, 13, 200, https://doi.org/10.3390/geosciences13070200, 2023.

Omran, A., Fahmida, K., Schröder, D., Arnous, M. O., El-Rayes, A. E., and Hochschild, V.: GIS-based rockfall hazard zones modeling along the coastal Gulf of Aqaba Region, Egypt, Earth Sci Inform, 14, 691–709, https://doi.org/10.1007/s12145-021-00580-y, 2021.

https://doi.org/10.5194/nhess-2024-85
Preprint. Discussion started: 24 July 2024

Othman, A., Shaaban, F., Abotalib, A. Z., El-Saoud, W. A., Gabr, S. S., Habeebullah, T., and Hegazy, D.: Hazard Assessment of Rockfalls in Mountainous Urban Areas, Western Saudi Arabia, Arab J Sci Eng, 46, 5717–5731, https://doi.org/10.1007/s13369-020-05098-x, 2021.

Paredes, C., Sarro, R., and Ramos, M.: Estimación preliminar de los alcances por caída de bloques en la sierra de La Cabrera, Madrid, España, Revista mexicana de ciencias geologicas, 32, 475–491, 2015.

Pérez-Rey, I., Riquelme, A., González-deSantos, L. M., Estévez-Ventosa, X., Tomás, R., and Alejano, L.: A multi-approach rockfall hazard assessment on a weathered granite natural rock slope, Landslides, https://doi.org/10.1007/s10346-019-01208-5, 2019.

Pfeiffer, T. J.: Application of Rockfall Simulation to Risk Analysis, 70th Highway Geology SymposiumHighway Geology Symposium, 2019.

Robiati, Eyre, Vanneschi, Francioni, Venn, and Coggan: Application of Remote Sensing Data for Evaluation of Rockfall Potential within a Quarry Slope, IJGI, 8, 367, https://doi.org/10.3390/ijgi8090367, 2019.

Rossi, M. and Reichenbach, P.: LAND-SE: a software for statistically based landslide susceptibility zonation, version 1.0, Geoscientific Model Development, 9, 3533–3543, https://doi.org/10.5194/gmd-9-3533-2016, 2016.

Rossi, M., Guzzetti, F., Reichenbach, P., Mondini, A. C., and Peruccacci, S.: Optimal landslide susceptibility zonation based on multiple forecasts, Geomorphology, 114, 129–142, https://doi.org/10.1016/j.geomorph.2009.06.020, 2010.

Rossi, M., Sarro, R., Reichenbach, P., and Mateos, R. M.: Probabilistic identification of rockfall source areas at regional scale in El Hierro (Canary Islands, Spain), 2020.

Rossi, M., Bornaetxea, T., and Reichenbach, P.: LAND-SUITE V1.0: a suite of tools for statistically based landslide susceptibility zonation, Geoscientific Model Development, 15, 5651–5666, https://doi.org/10.5194/gmd-15-5651-2022, 2022.

Santangelo, M., Marchesini, I., Bucci, F., Cardinali, M., Cavalli, M., Crema, S., Marchi, L., Alvioli, M., and Guzzetti, F.: Exposure to landslides in rural areas in Central Italy, Journal of Maps, 0, 1–9, https://doi.org/10.1080/17445647.2020.1746699, 2020.

Santos, P. P., Reyes-Carmona, C., Pereira, S., Sarro, R., Martínez-Corbella, M., Coll-Ramis, M. À., Zêzere, J. L., and Mateos, R. M.: Seasonal rockfall risk analysis in a touristic island: Application to the Tramuntana Range (Mallorca, Spain), International Journal of Disaster Risk Reduction, 101, 104264, https://doi.org/10.1016/j.ijdrr.2024.104264, 2024.

Sarro, R., Mateos, R. M., García-Moreno, I., Herrera, G., Reichenbach, P., Laín, L., and Paredes, C.: The Son Poc rockfall (Mallorca, Spain) on the 6th of March 2013: 3D simulation, Landslides, 11, 493–503, https://doi.org/10.1007/s10346-014-0487-8, 2014.

Sarro, R., Riquelme, A., García-Davalillo, J. C., Mateos, R. M., Tomás, R., Pastor, J. L., Cano, M., and Herrera, G.: Rockfall simulation based on UAV photogrammetry data obtained during an emergency declaration: Application at a cultural heritage site, https://doi.org/10.3390/rs10121923, 2018.

Sarro, R., Mateos, R. M., Reichenbach, P., Aguilera, H., Riquelme, A., Hernández-Gutiérrez, L. E., Martín, A., Barra, A., Solari, L., Monserrat, O., Alvioli, M., Fernández-Merodo, J. A., López-Vinielles, J., and Herrera, G.: Geotechnics for rockfall assessment in the volcanic island of Gran Canaria (Canary Islands, Spain), Journal of Maps, 16, 605–613, https://doi.org/10.1080/17445647.2020.1806125, 2020.

https://doi.org/10.5194/nhess-2024-85
Preprint. Discussion started: 24 July 2024

Sarro, R., Pérez-Rey, I., Tomás, R., Alejano, L. R., Hernández-Gutiérrez, L. E., and Mateos, R. M.: Effects of Wildfire on Rockfall Occurrence: A Review through Actual Cases in Spain, Applied Sciences, 11, 2545, https://doi.org/10.3390/app11062545, 2021.

Scavia, C., Barbero, M., Castelli, M., Marchelli, M., Peila, D., Torsello, G., and Vallero, G.: Evaluating Rockfall Risk: Some Critical Aspects, Geosciences, 10, 98, https://doi.org/10.3390/geosciences10030098, 2020.

Straub, D. and Schubert, M.: Modeling and managing uncertainties in rock-fall hazards, Georisk: Assessment and Management of Risk for Engineered Systems and Geohazards, 2, 1–15, https://doi.org/10.1080/17499510701835696, 2008.

Tehrani, F. S., Calvello, M., Liu, Z., Zhang, L., and Lacasse, S.: Machine learning and landslide studies: recent advances and applications, Nat Hazards, 114, 1197–1245, https://doi.org/10.1007/s11069-022-05423-7, 2022.

Wang, L.-J., Guo, M., Sawada, K., Lin, J., and Zhang, J.: A comparative study of landslide susceptibility maps using logistic regression, frequency ratio, decision tree, weights of evidence and artificial neural network, Geosci J, 20, 117–136, https://doi.org/10.1007/s12303-015-0026-1, 2016.

Wang, X., Liu, H., and Sun, J.: A New Approach for Identification of Potential Rockfall Source Areas Controlled by Rock Mass Strength at a Regional Scale, Remote Sensing, 13, 938, https://doi.org/10.3390/rs13050938, 2021.

Yan, J., Chen, J., Tan, C., Zhang, Y., Liu, Y., Zhao, X., and Wang, Q.: Rockfall source areas identification at local scale by integrating discontinuity-based threshold slope angle and rockfall trajectory analyses, Engineering Geology, 313, 106993, https://doi.org/10.1016/j.enggeo.2023.106993, 2023.

Yang, X., Zhang, G., Yu, Y., Yu, Q., Lei, M., and Ding, B.: Factors Influencing the Coefficient of Restitution in Rockfall Impacts, Natural Hazards Review, 22, 04021024, https://doi.org/10.1061/(ASCE)NH.1527-6996.0000454, 2021.

Žabota, B., Repe, B., and Kobal, M.: Influence of digital elevation model resolution on rockfall modelling, Geomorphology, 328, 183–195, https://doi.org/10.1016/j.geomorph.2018.12.029, 2019.

Zhan, J., Yu, Z., Lv, Y., Peng, J., Song, S., and Yao, Z.: Rockfall Hazard Assessment in the Taihang Grand Canyon Scenic Area Integrating Regional-Scale Identification of Potential Rockfall Sources, Remote Sensing, 14, 3021, https://doi.org/10.3390/rs14133021, 2022.

https://doi.org/10.5194/nhess-2024-85
Preprint. Discussion started: 24 July 2024

Natural Hazards and Earth System Sciences
Discussions

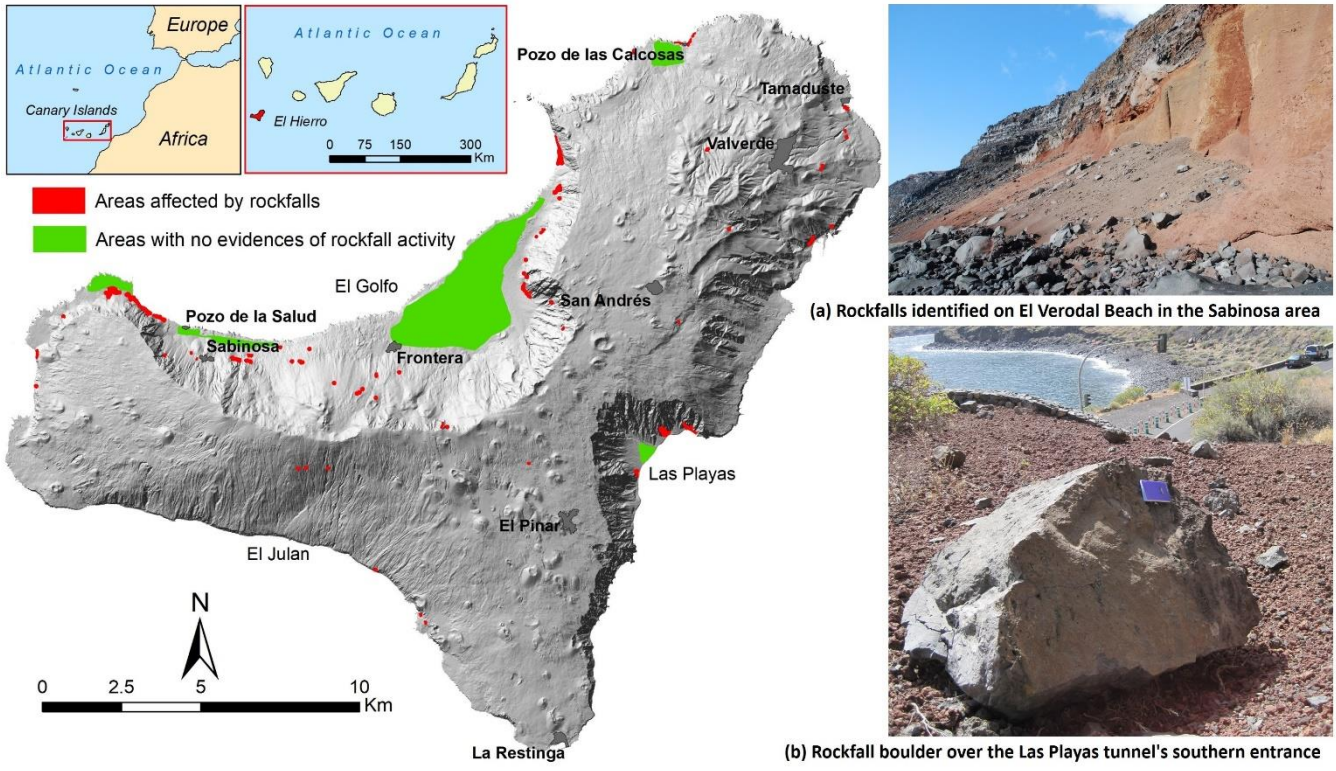

Figure 1: Areas used to classify and validate the simulated rockfall runout.

https://doi.org/10.5194/nhess-2024-85
Preprint. Discussion started: 24 July 2024

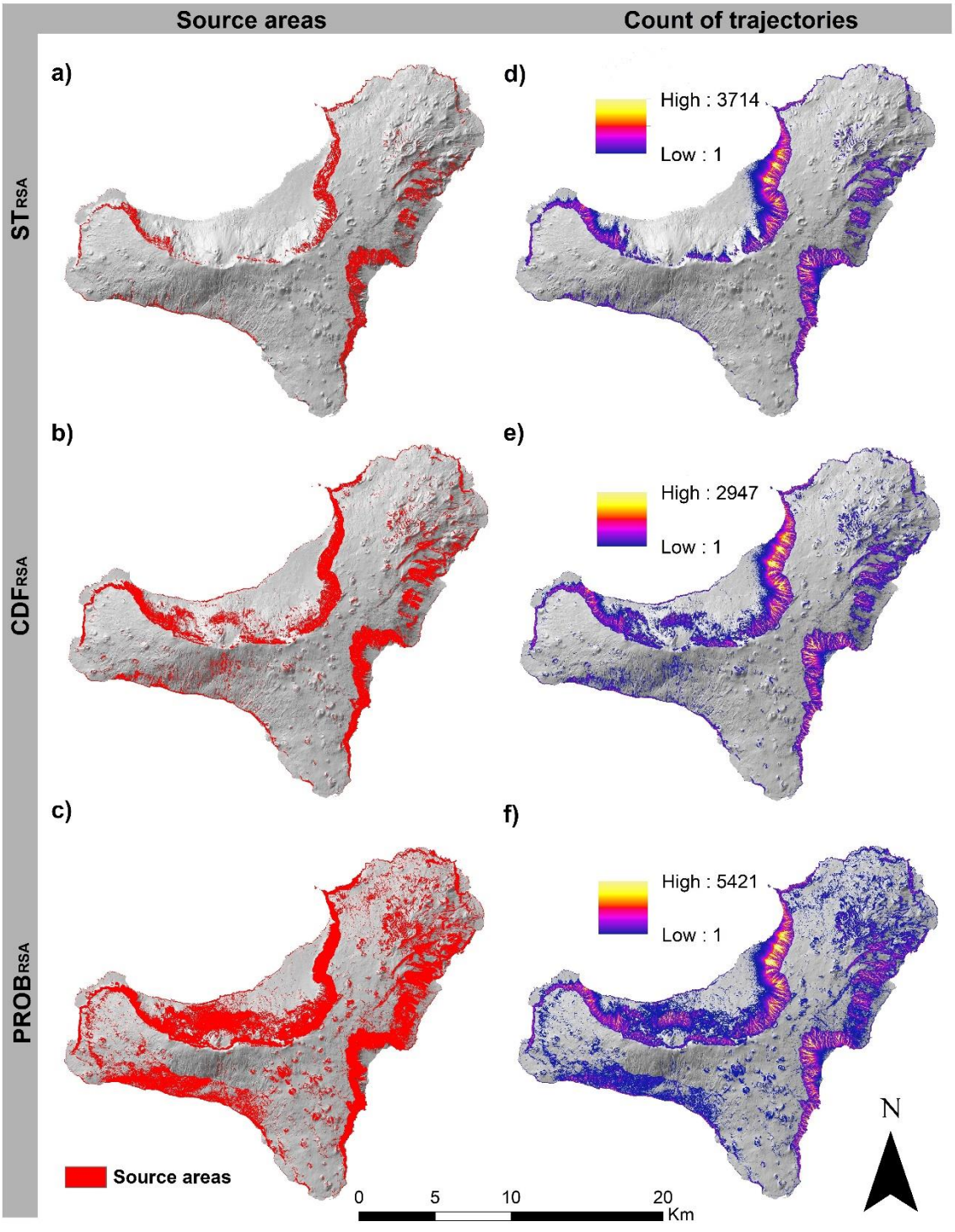

Figure 2: The maps show results of the source areas identified using the 3 different approaches (a, ST_{RSA}; b, $CDF_{RSA;}$ and c, $PROB_{RSA}$) and the cumulative frequency of rockfall trajectories counts for each source area identification approach (d, e, f).

https://doi.org/10.5194/nhess-2024-85
Preprint. Discussion started: 24 July 2024

Natural Hazards and Earth System Sciences
Discussions

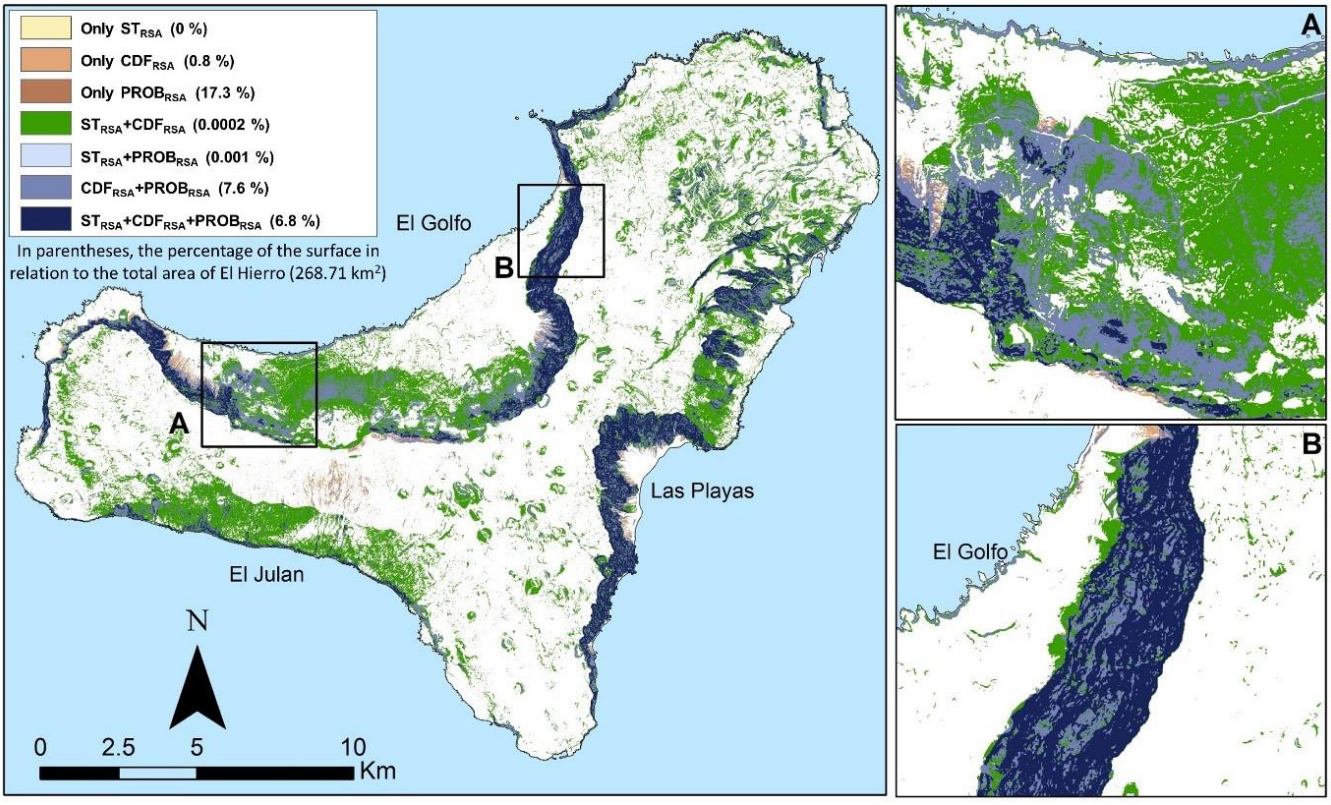

Figure 3: The map shows results of the spatial comparison of the source areas identified using the 3 different approaches (i.e., ST_{RSA}, CDF_{RSA} and $PROB_{RSA}$).

https://doi.org/10.5194/nhess-2024-85
Preprint. Discussion started: 24 July 2024

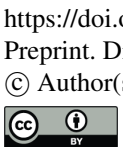

Natural Hazards and Earth System Sciences
Discussions

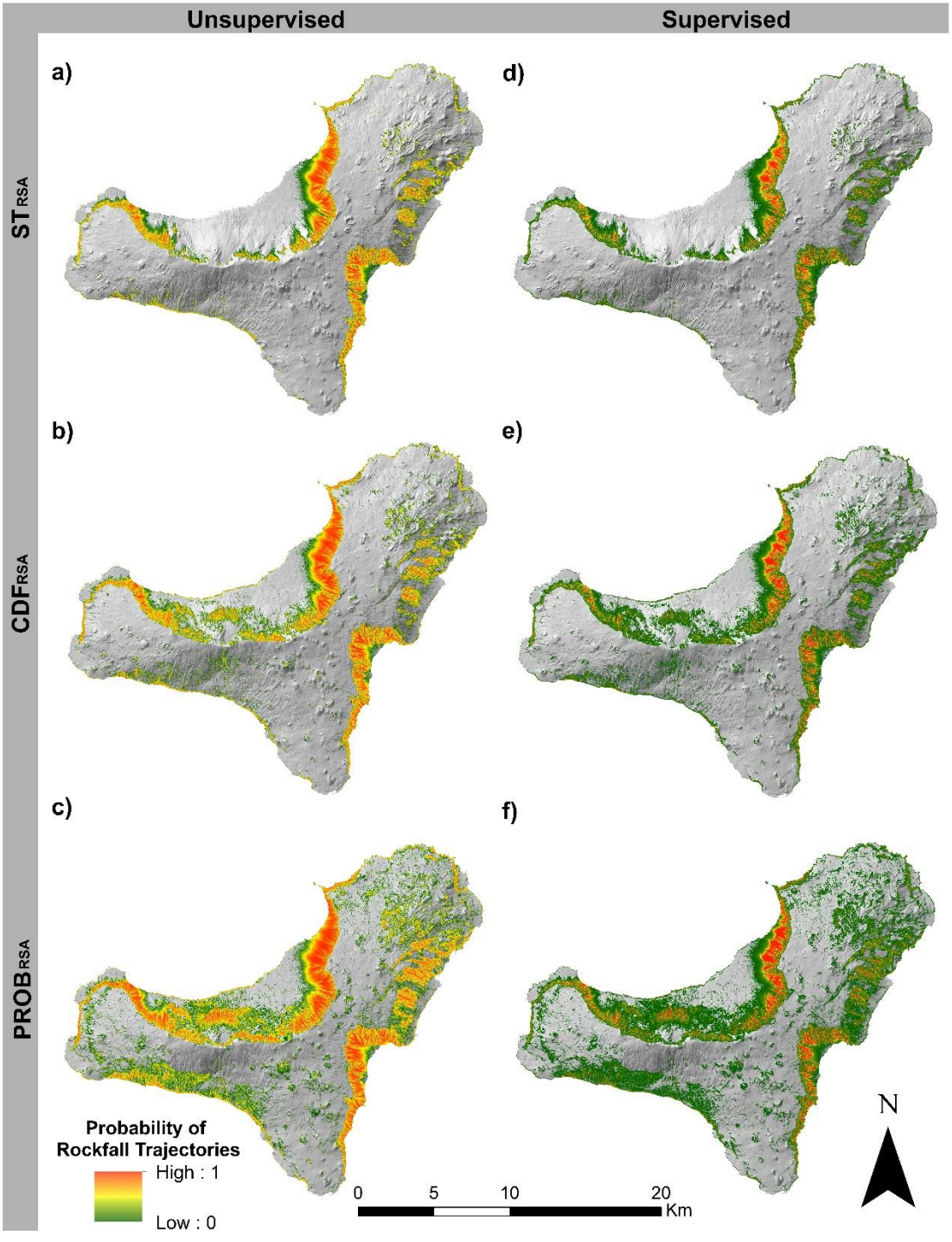

Figure 4: Probabilistic susceptibility maps derived from the application of unsupervised (a, b, c) and supervised (d, e, f) ECDFs (Figure 5).

https://doi.org/10.5194/nhess-2024-85
Preprint. Discussion started: 24 July 2024

Natural Hazards and Earth System Sciences
Discussions

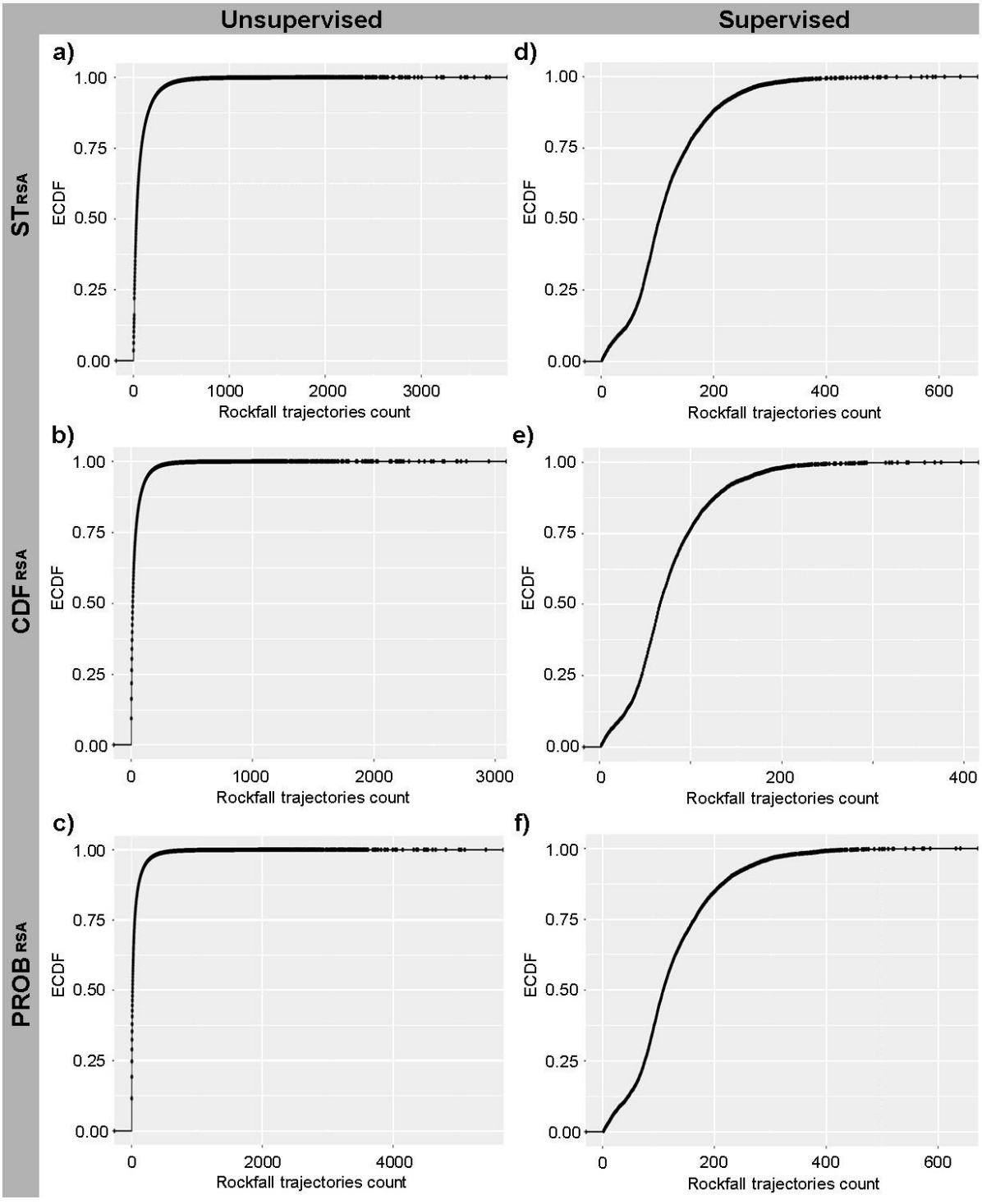

Figure 5: Unsupervised (a, b, c) and supervised (d, e, f) ECDF functions derived for outputs obtained for the different source areas identification methods.

https://doi.org/10.5194/nhess-2024-85
Preprint. Discussion started: 24 July 2024

Natural Hazards and Earth System Sciences
Discussions

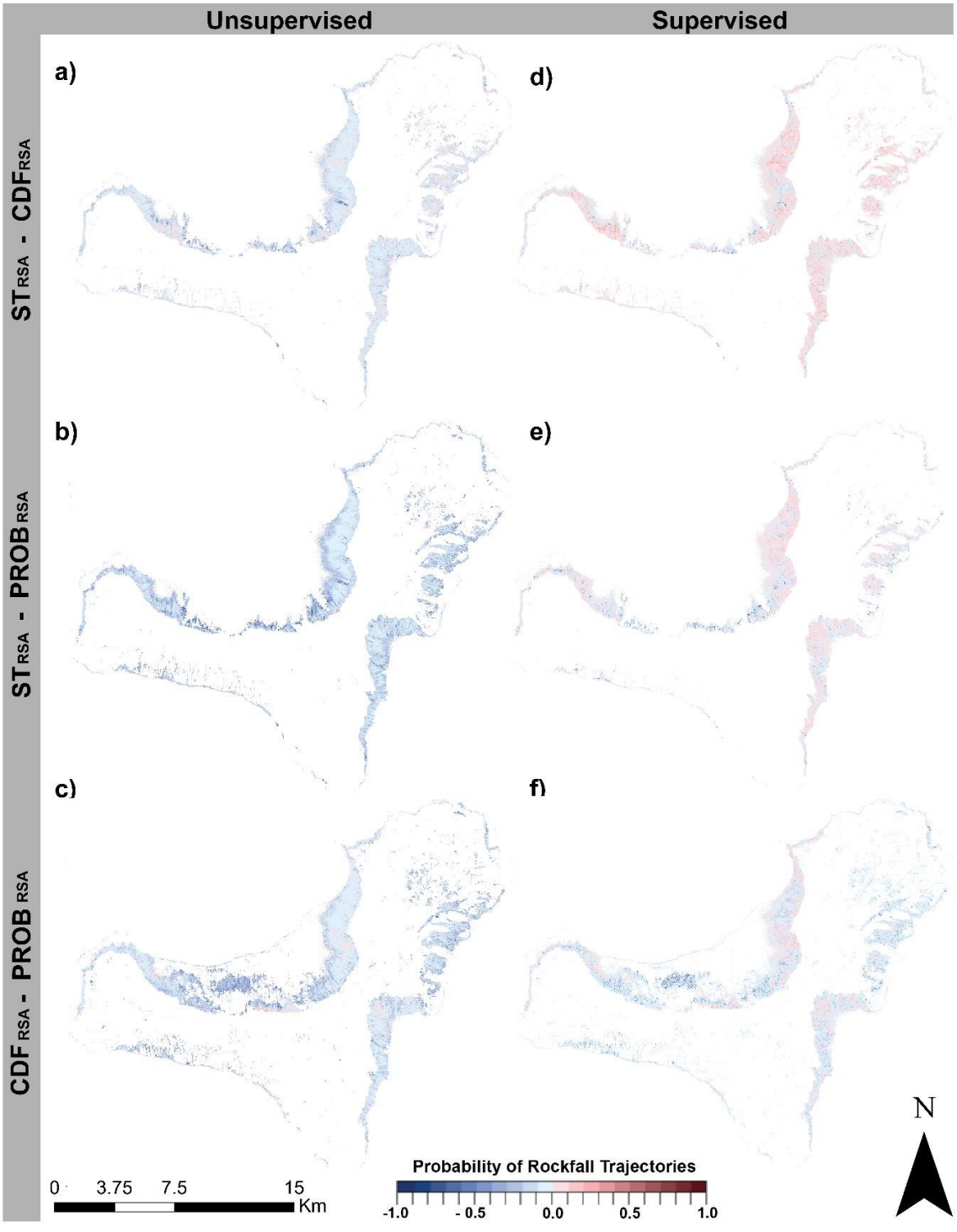

Figure 6: Maps of the pairwise differences of susceptibility maps obtained for different source areas identification methods (row wise), and diversified classification method used (column wise).

https://doi.org/10.5194/nhess-2024-85
Preprint. Discussion started: 24 July 2024

Natural Hazards and Earth System Sciences
Discussions

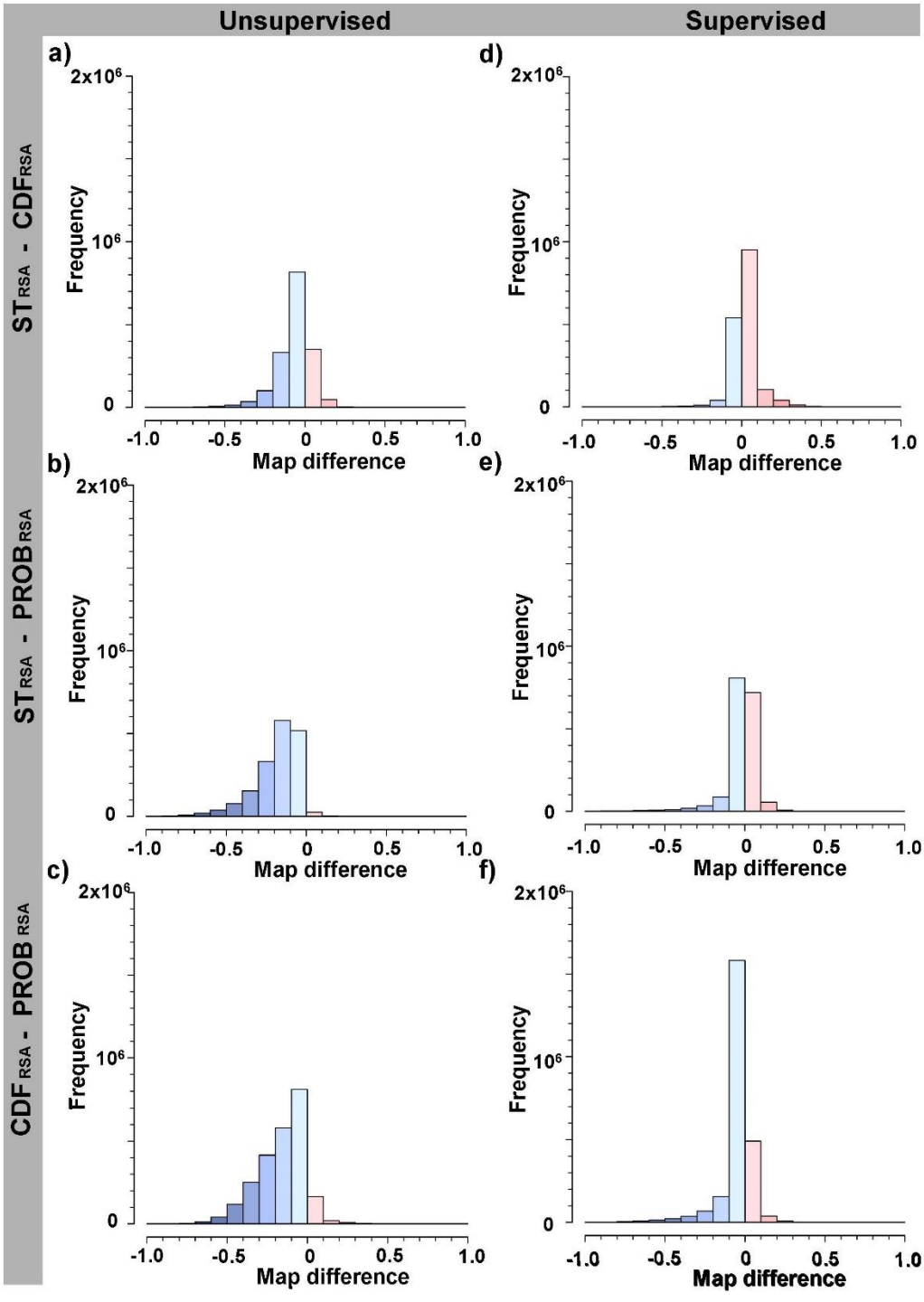

590 Figure 7: Histograms of the pairwise differences of susceptibility maps obtained for different source areas identification methods (row wise) and diversified classification method used (column wise).

https://doi.org/10.5194/nhess-2024-85
Preprint. Discussion started: 24 July 2024

Natural Hazards and Earth System Sciences
Discussions

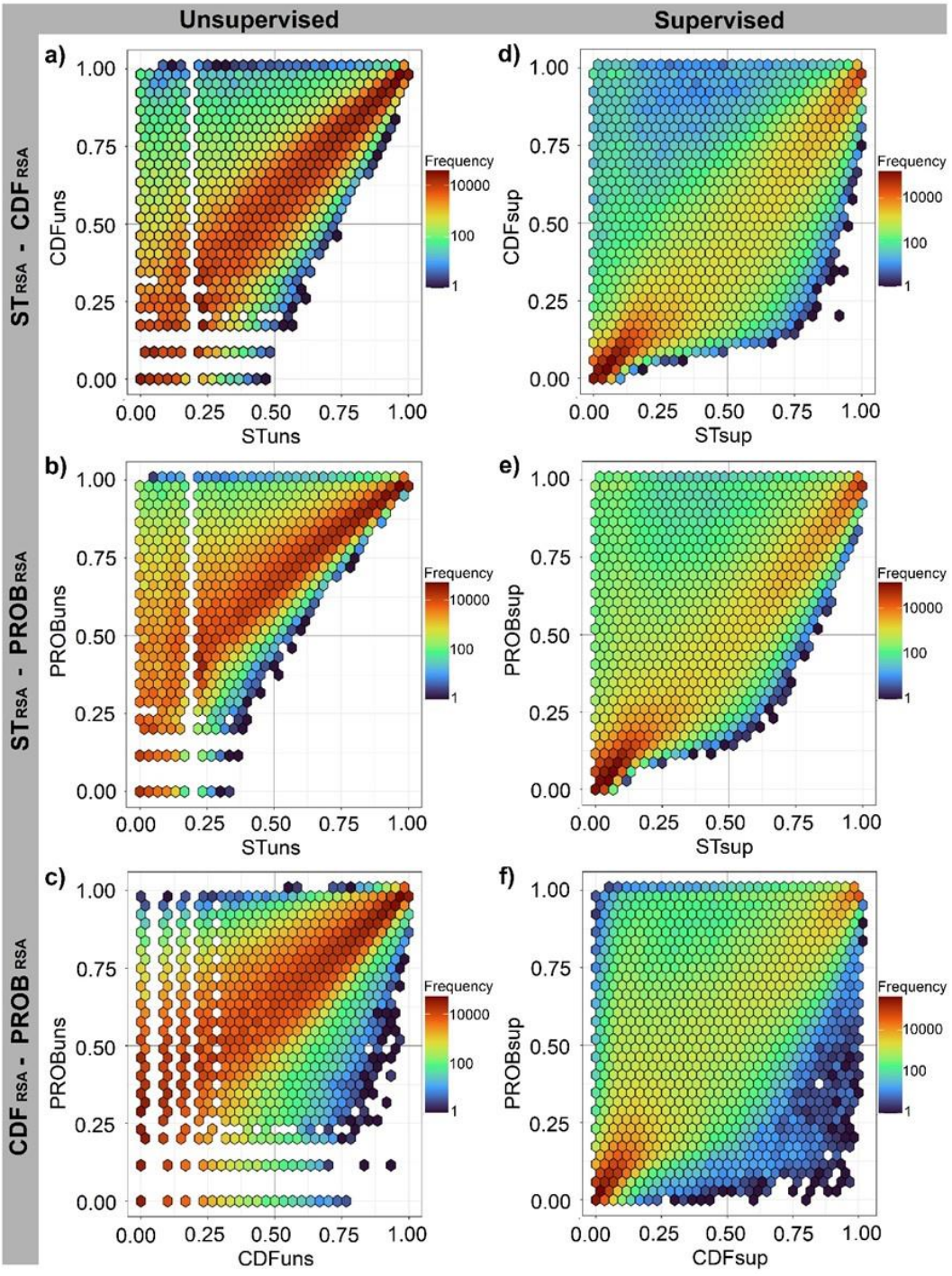

Figure 8: 2D hexagonal bin count heat maps derived for the different pairs of susceptibility maps obtained applying unsupervised (a, b, c) and supervised (d, e, f) ECDFs. Dark reddish shades indicate a higher frequency of measurements within the corresponding hexagon.

https://doi.org/10.5194/nhess-2024-85
Preprint. Discussion started: 24 July 2024

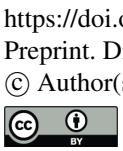

Natural Hazards and Earth System Sciences
Discussions

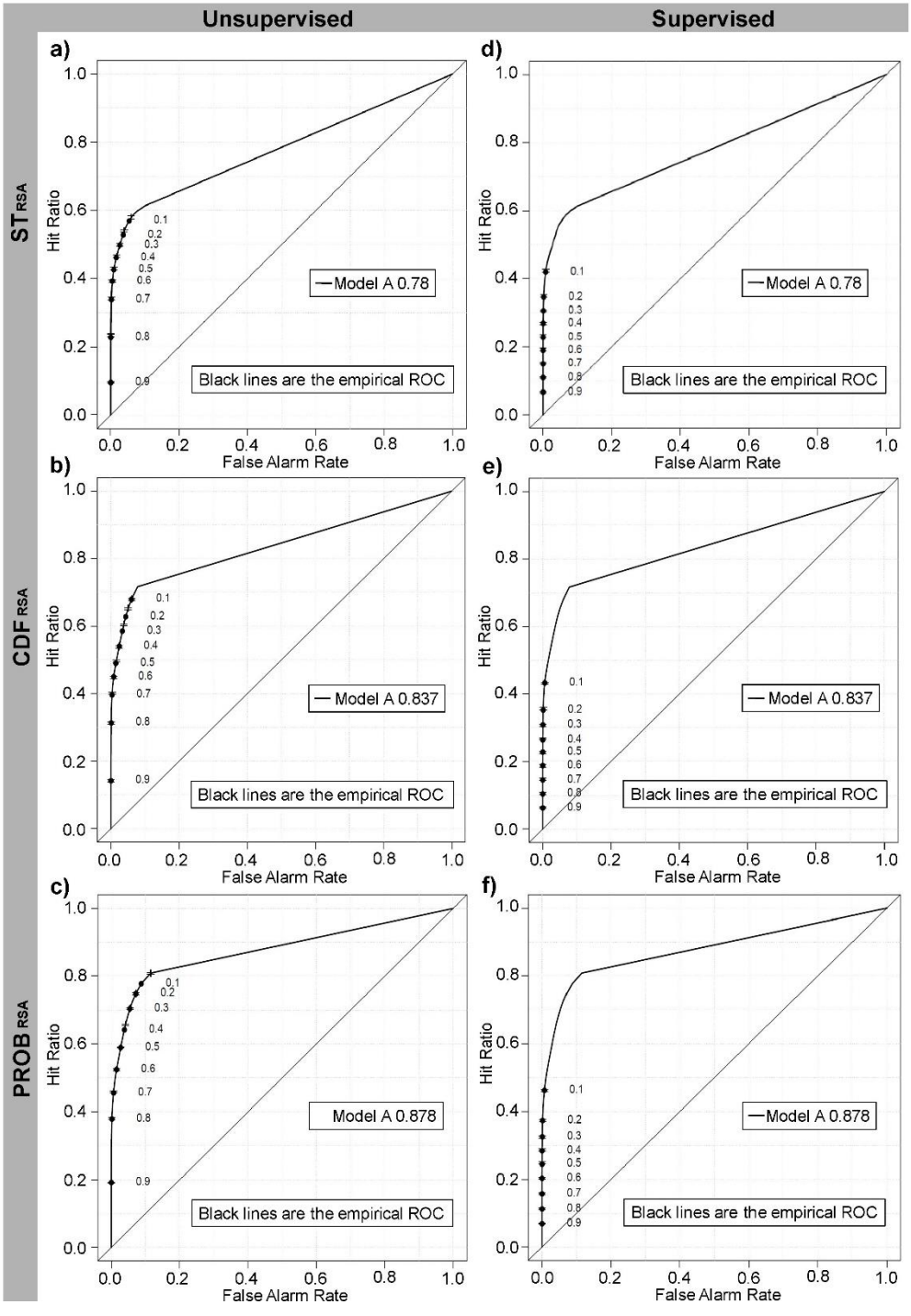

Figure 9: ROC plots and corresponding AUC_{ROC} values derived for the six susceptibility maps shown in figure 4. Point shows values of the Hit Rate (also referred as True Positive Rate or Sensitivity) and False Alarm Rate (also referred as False Positive Rate equivalent to 1 - Specificity) for a set of probability threshold reference values.

https://doi.org/10.5194/nhess-2024-85
Preprint. Discussion started: 24 July 2024

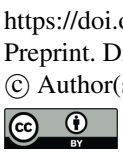

Natural Hazards and Earth System Sciences
Discussions

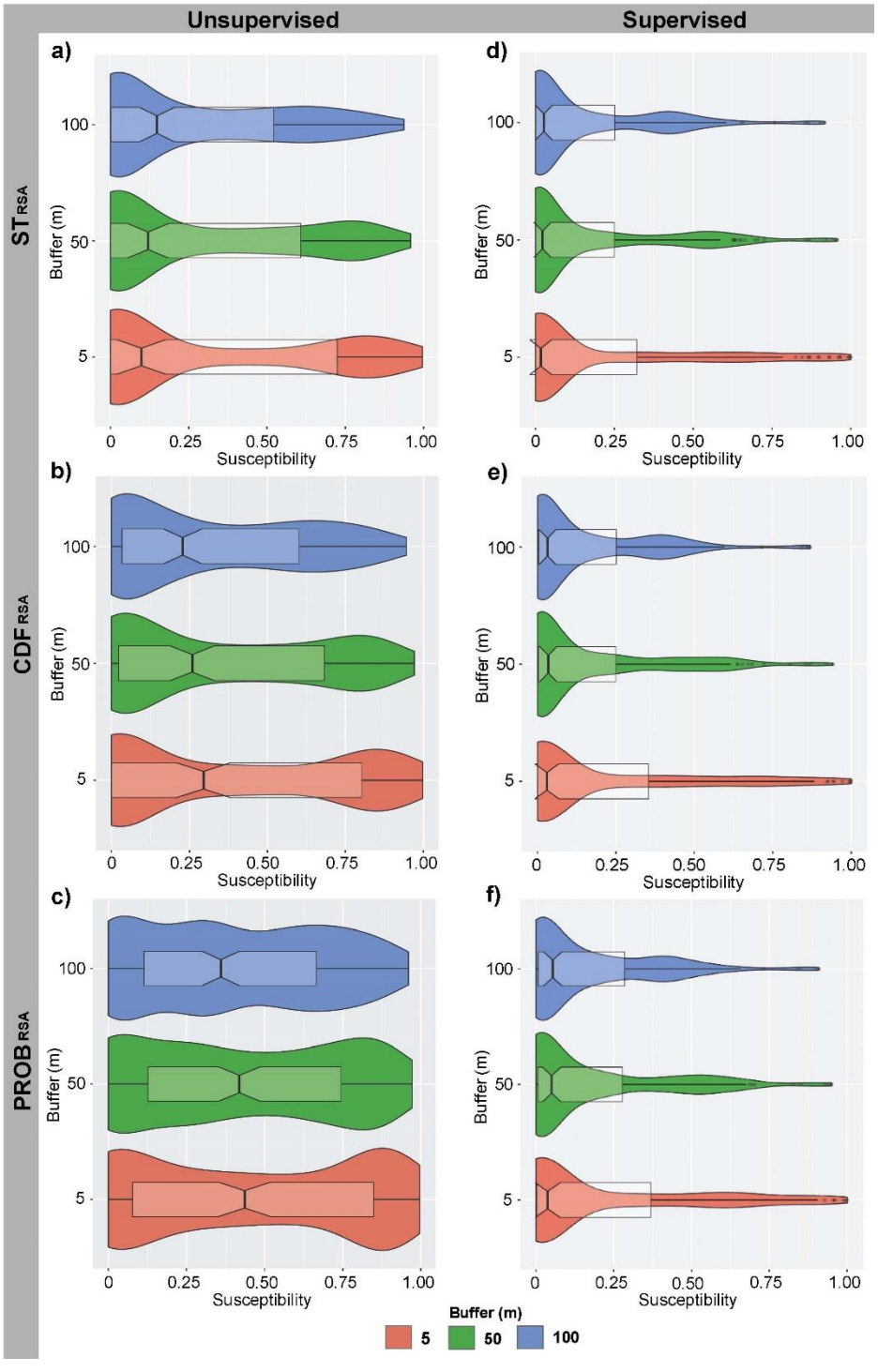

Figure 10: Violin and boxplots derived for the average values of susceptibility within buffers defined around rockfall boulder locations. Plots correspond to the six susceptibility maps shown in Figure 4.

https://doi.org/10.5194/nhess-2024-85
Preprint. Discussion started: 24 July 2024

Natural Hazards and Earth System Sciences
Discussions

Table 1: The table shows the spatial dimensions of source areas identified by the 3 approaches (i.e., ST_{RSA}, CDF_{RSA} and $PROB_{RSA}$).

Source areas maps	Total *(pixel)*	Area *(km^2)*	% Of Hierro island *(268,71 km^2)*
ST_{RSA}	727603	18.19	6.8%
CDF_{RSA}	1628048	40.70	15.1%
$PROB_{RSA}$	3399686	84.99	31.6%

https://doi.org/10.5194/nhess-2024-85
Preprint. Discussion started: 24 July 2024

Table 2: This table shows the differences of the spatial distribution of source areas as identifies by the 3 approaches (i.e., ST_{RSA}, CDF_{RSA} and $PROB_{RSA}$). It also identifies the geotechnical classes in the difference (1: Soft soils; 2: Hard soils; 3: Soft rocks; 4: Hard rocks; 5: Very hard rocks).